Available online at www.sciencedirect.com
ScienceDirect
Journal of the European Ceramic Society 32 (2012) 211–218
www.elsevier.com/locate/jeurceramsoc

Effect of HCl concentration on the sintering behavior of 8 mol% Y_2O_3 stabilized ZrO_2 deposits produced by electrophoretic deposition (EPD)

Fangwei Guo, Athar Javed, Ian P. Shapiro, Ping Xiao *

Materials Science Centre, School of Materials, University of Manchester, Grosvenor Street, Manchester, M1 7HS, UK

Received 3 June 2011; received in revised form 3 August 2011; accepted 7 August 2011
Available online 30 August 2011

Abstract

In this work, we have investigated the effect of HCl concentration and particle packing on the sintering behavior of 8 mol% yttria-stabilized-zirconia (8YSZ) deposits. 8YSZ deposits were fabricated by electrophoretic deposition (EPD). For 8YSZ coatings, it was found that the concentration of HCl in the EPD suspension significantly influences the neck size to grain size ratio. High neck size to grain size ratio (0.8 ± 0.03) was found in the sintered 0.8 HCl coating. The grain growth was observed to depend on the initial particle packing in the green coating. The effect of chloride ions on the grain and neck growth as well as elemental segregation within the 8YSZ is investigated using photoelectron spectroscopy (XPS) which confirmed the presence of chloride ions in green and sintered 8YSZ coatings. This was later confirmed using high-resolution transmission electron microscopy (HRTEM) and thermal analysis techniques. It was found that the presence of chloride ions induced an increase in the oxygen vacancy concentration at the grain boundaries. High oxygen vacancy concentration in the grain boundaries could promote neck growth of 8YSZ.

Keywords: HCl; YSZ; EPD; Sintering; Oxygen vacancy

1. Introduction

Yttria-stabilized cubic zirconia (Y-CSZ) is of interest for use in various electrochemical devices, such as fuel cells and oxygen sensors due to its excellent toughness, high mechanical resistance, high melting point and good ionic conductivity.[1–3] Depending on the application, electric and mechanical properties can be controlled by composition, processing conditions and the sintering cycle. Electrophoretic deposition (EPD) is a low cost method to produce coatings and has gained much attention due to easy manipulation of the microstructure and thickness of ceramic coatings on complex-shaped substrates in comparison with plasma spraying, chemical vapor deposition and physical vapor deposition.[4–8] Sintering is the final densification stage of EPD coatings. During the sintering process, neck formation, pore contraction and grain growth play an important role in defining the mechanical and electrical properties of the final product.[9–11] It is known that the growth of necks at particle junctions can occur by surface diffusion as well as by grain-boundary diffusion.[12,13] Kuczynski's[13] theoretical predictions gave an insight into the role of surface diffusion in the formation of necks between particles during early stage sintering. In order to increase the neck area, various approaches have been adopted including mixing powders with multimodal particle size distribution and use of dopants that enhance surface diffusion.[14]

Grain growth during sintering in yttria-stabilized-zirconia polycrystals (Y-TZP) and Y-CSZ has been investigated extensively.[15–18] The extent, to which Y^{3+} ions segregate to the grain boundaries of YSZ has a decisive influence on grain growth. Matsui et al.[19] systematically investigated the grain-boundary structure and microstructure development mechanism in 2–8 mol% yttria-stabilized zirconia polycrystals using high-resolution transmission electron microscopy (HRTEM) and energy dispersive X-ray spectroscopy (EDS). They observed that low Y^{3+} ions segregation occurred in the 8 mol% YSZ as compared with 3 mol% YSZ and 2 mol% YSZ which had greatest Y^{3+} ion segregation. It has also been reported that residual chlorine from the precursor chloride salts such as YCl_3 and $ZrCl_4$ can negatively affect the surface properties and crystallization of the ZrO_2 matrix.[20–22] Moreover, a small leaching of minor constituents such as the stabilizing agent (yttria in this work) in acid solution promotes dramatic degradation. The monoclinic

* Corresponding author. Tel.: +440161 3065941; fax: +440161 3063586.
E-mail address: ping.xiao@manchester.ac.uk (P. Xiao).

0955-2219/$ – see front matter © 2011 Elsevier Ltd. All rights reserved.
doi:10.1016/j.jeurceramsoc.2011.08.011

phase transformation started to appear at moderate acidic pH of about 3.5–4 in the HF, HCl and HNO_3 solutions.[23] Lawson et al.[24] found that up to 80% monoclinic phase was found after acidic corrosion of dense samples of 3Y-TZP, which was predominantly controlled by hydrothermal degradation at 180 °C. Readey and Readey[25] reported that ZrO_2 grain growth is much more rapid in an HCl atmosphere than in air due to enhanced vapour transport via volatile chloride species. On the contrary, Raether and Springer[26] observed fast densification and rapid neck formation in Al_2O_3, while Suzuki et al.[27] observed fast densification and rapid neck formation in MgO, washed in a concentrated HCl solution before sintering.[28]

In this study, we have investigated how the HCl concentration of the EPD suspension and the green coatings particle packing effects the sintering behavior of 8 mol% yttria stabilized zirconia (8YSZ) coatings. 8YSZ coatings were deposited on Fecralloy substrates from suspensions with various HCl concentrations using electrophoretic deposition (EPD). For different HCl concentration, the neck and grain growth in coatings sintered at different temperatures (1150–1500 °C) for 2 h were examined using scanning electron microscopy (SEM), X-ray diffraction (XRD), thermal analysis, photoelectron spectroscopy (XPS) and high-resolution transmission electron microscopy (HRTEM).

2. Experimental procedure

For electrophoretic deposition (EPD), suspensions were prepared from commercially available (Pi-KEM Ltd., UK) YSZ powder (HSY-8, purity >99%, cubic phase). A mixture of ethanol (Et-OH, >99%, Sigma–Aldrich, UK) and acetyl-acetone (ACAC, >99%, Sigma–Aldrich, UK) with a molar ratio 7:4, was used as the solvent for all suspensions. HCl (0.1 mol/L in distilled water) was used to adjust the particle surface charge in suspensions. 20 g/L of YSZ was dispersed in the solvent with 5 minutes ultrasonic treatment (22.5 kHz, Microson XL 2000, Misonix Inc., Farmingdale, NY, USA). This suspension was used for EPD with a constant D.C. electric field of 50 V cm^{-1} (E863, Consort, Belgium) for between 1 min and 5 min. Fecralloy sheet ($FeCr_{22}Al_{4.8}Si_{0.3}Y_{0.3}$ [wt.%]; Good Fellow Ltd., Cambridge, UK) was used as the substrate. The distance between platinum electrode (anode) and Fecralloy foil (cathode) was ~10 mm. After overnight drying in ambient air, green coatings were removed from the substrates and sintered at 1150 °C. High sintering temperatures (>1200 °C) will degrade the mechanical performance of Fecralloy, hence 1150 °C was chosen to maintain practical relevance. In this study free standing green coating was used to avoid confounding effects due to constrained sintering. For convenience, it should be noted that the 0 HCl, 0.2 HCl, 0.5 HCl and 0.8 HCl coatings represent the free standing coatings fabricated in the 20 g/L YSZ suspension with HCl concentration of 0 mM, 0.2 mM, 0.5 mM and 0.8 mM HCl, respectively.

Before EPD coating, the average particle size of the YSZ powder was about 0.20 ± 0.05 μm as measured using scanning electron microscopy (SEM, XL30 FEG, Philips, The Netherlands). However, most particles were agglomerated. Using laser diffraction (Malvern, Micro Trac X100, Worcestershire, UK), the modal agglomerate size of particles was found to be 0.27 μm with 90% of the aggregates smaller than 1 μm.

The density of the green and sintered deposits was calculated from the weight and dimensions of all coatings. The grain size was estimated using the mean linear intercept technique (from SEM images) by taking the mean grain size as equal to 1.5 times the mean intercept, as described in Ref. 29. The mean neck size was estimated from the SEM images by taking measurements from 50 to 100 grains. Thermal analysis of the powder was conducted using a NETZSCH STA 449C thermal analyzer to obtain thermo-gravimetric (TG) and differential scanning calorimetric (DSC) data. Both TG and DSC were carried out in continuous scan mode with heating and cooling rates of 3 °C/min under a flowing air atmosphere. The testing powder was ground from free standing YSZ-EPD green deposits. X-ray diffraction (XRD; PW1830/40, Philips, The Netherlands) with Cu Kα radiation (wavelength, $\lambda = 1.5406$ Å) was used to characterize the starting powder and sintered deposits. For detailed composition analysis, X-ray photoelectron spectroscopy (XPS, Axis Ultra) with monochromatic Al Kα radiation (of energy $E = 1486.6$ eV) was used. The surface C1s photoemission at $E = 284.6$ eV[30] was used as a reference binding energy. The surface composition was then calculated utilizing the atomic sensitivity factors of all surface elements as described in Ref. 31. The grain boundary structure and segregation was observed by analytical transmission electron microscopy (TEM/STEM, Tecnai^{TM} G^2 F30 U-TWIN). Semi-quantitative analysis of Y^{3+}, Zr^{4+} and O^{2-} segregation at grain boundaries was performed using scanning TEM (STEM) mode with a probe size of about 2 nm and energy dispersive X-ray spectroscopy (EDS) system. For each sample, three grain boundaries were analyzed. For TEM study, the samples were prepared (adopting the method described in Ref. 32) by cutting the cross-section of EPD-sintered 8YSZ coatings using a focused ion beam (FIB, FEI Nova 600 Dual Beam System).

3. Results

3.1. Density and grain size

Fig. 1(a) shows the relative density as a function of HCl concentration for coatings sintered at 1150 °C. From Fig. 1(a), it can be seen that the relative green densities of coatings prepared with suspensions of 0.2 HCl, 0.5 HCl and 0.8 HCl concentrations were nearly identical. However, for green coatings without HCl the relative density was ~15% lower than those prepared with HCl The green density of coatings deposited using EPD mainly depends on the zeta potential of charged particles in suspension. Our previous work[33] found that the zeta potential of 0 HCl suspension was lower than that of 0.2, 0.5 and 0.8 HCl suspensions, which led to loose particle packing in these green coatings. After sintering at 1150 °C, the coatings had slightly higher densities than that of the green coatings over the whole range of HCl concentration studied. Further, it was observed that the relative density of the sintered coating followed a similar trend as seen for the green coatings (Fig. 1(a)). This was expected as the sintered density of coatings substantially depends on green density of coatings.

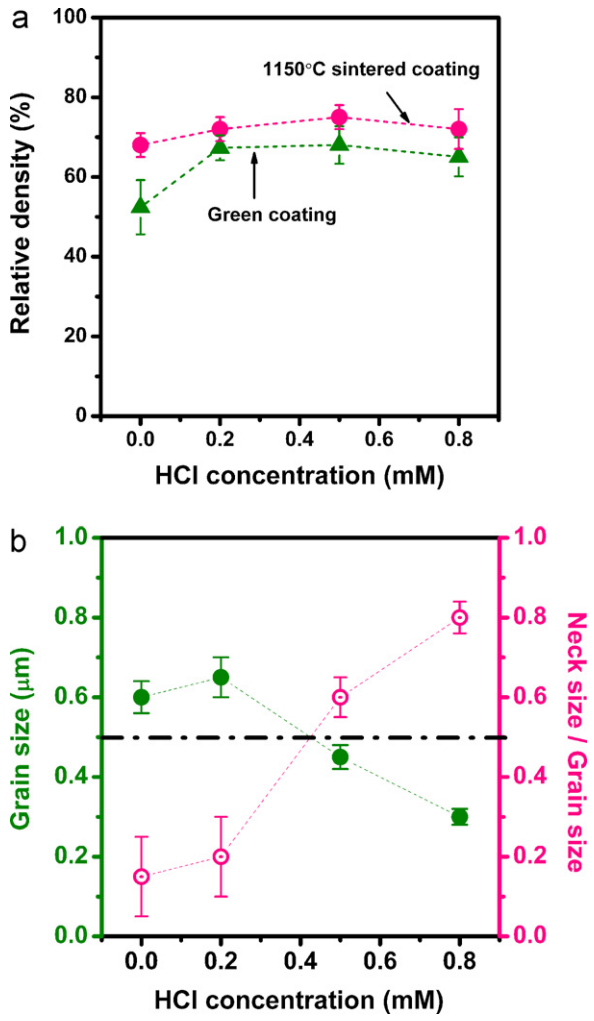

Fig. 1. (a) Relative density as a function of HCl concentration for green and sintered 8YSZ coatings; (b) the grain size and neck size to grain size ratio (*X*/*D*) as a function of HCl concentration for YSZ coating sintered at 1150 °C for 2 h.

Fig. 1(b) shows grain size as a function of HCl concentration for 8YSZ coatings sintered at 1150 °C for 2 h. Above 0.2 mM HCl concentration, the grain size decreases with the increase in HCl concentration. Fig. 1(b) also shows the neck size to grain size ratio (X/D) as a function of HCl concentration. The SEM image shown in Fig. 2(a) defines the neck size for all sintered coatings. It is an intercept between two adjacent grains (see black lines in Fig. 2(a)). For sintered coatings, the mean neck size data were averaged over 50 measurements. It was found that the mean neck size to grain size ratio (*X*/*D*) increased with increases in HCl concentration above 0.2 mM. The largest grain size (0.65 ± 0.05 μm) was observed for 0.2 HCl coatings, while 0.8 HCl coatings had the smallest grain size (0.3 ± 0.02 μm). For 0.8 mM HCl concentration, high neck size to grain size ratio (0.8 ± 0.03) was observed (Fig. 1(b)). From the data shown in Fig. 1(b), it can be concluded that the HCl concentration has a significant effect on both grain size and neck size to grain size ratio with transition between 0.2 and 0.5 mM HCl concentration.

Fig. 2(b)–(d) shows typical surface morphologies of green coatings (Fig. 2(b)), sintered 0.2 HCl coating (Fig. 2(c)) and sintered 0.8 HCl coatings (Fig. 2(d)) respectively. Substantial grain growth was observed in the sintered 0.2 HCl coating compared with the green coating (Fig. 2(b)) and the sintered 0.8 HCl coating (Fig. 2(d)). Further, it can be seen that the microstructure was not uniform for sintered 0.2 HCl coating. Fig. 2(c) shows that the microstructure consists of large crystallites surrounded by small particles in contrast to the 0.8 mM HCl concentration coating which has quite uniform microstructure (see Fig. 2(d)). The distinct microstructures for the sintered 0.2 HCl coating and 0.8 HCl coatings are attributed to the difference in suspension conductivity during EPD. Further details can be found in our previous work reported in Ref. 33.

3.2. Thermal analysis

Fig. 3 shows the TG and DSC curves as a function of calcination temperature for 8YSZ powder with 0 HCl and 0.5 HCl concentrations. The weight loss of raw (0 HCl) and 0.5 HCl powder increased with calcination temperature. For calcination temperature range 300–900 °C, the weight loss for 0.5 HCl powder was larger as compared to raw powder (Fig. 3). Moreover, there was a 0.05% weight fluctuation around 450–600 °C in both raw powder and 0.5 HCl YSZ powder. This corresponds to the minor endothermic peaks shown in the DSC curves for both 0 and 0.5 HCl 8YSZ powder. The large weight losses were attributed to decomposition of the residual organic solvent (ethanol and acetyl-acetone) decomposition and HCl evaporation as well as the removal of adsorbed gas and water.[34] An exothermic peak occurred at 1220 °C in both powders, which indicated that there was a phase transformation around this temperature (see DSC profile in Fig. 3. Room temperature XRD spectra (not shown) of 0 HCl, 0.2 HCl, 0.5 HCl and 0.8 HCl sintered YSZ coatings showed only (4 0 0) reflections ($2\theta = 73.6°$) corresponding to a single cubic phase with no evidence for the presence of monoclinic or tetragonal phases. This is consistent with the work reported in Refs. 21–23,35. No monoclinic or tetragonal phase formation was indicated by the DSC data (Fig. 3) for any of the coatings.

3.3. Composition analysis

Fig. 4(a) shows the XPS spectra of green and sintered 0 HCl and 0.5 HCl YSZ coatings. XPS spectra were collected to identify Zr_{3d}, reduced Zr^{4+} 3d, Y_{3d} and Cl_{2p} bands. The band positions and splitting of individual bands are also presented in Table 1. For the green 0.5 HCl coating, the binding energies of Zr_{3d} and Y_{3d} shifted ~1.7 eV and ~2.1 eV towards higher binding energy, respectively compared with the green 0 HCl coating. For the sintered 0.5 HCl coating, the binding energies of Zr_{3d} and Y_{3d} shifted ~1.2 eV and ~1.5 eV towards higher binding energy, respectively compared with the sintered 0 HCl coatings. The peaks in the range 170–178 eV correspond to the reduced Zr^{4+} 3d bands in lower valance state.[36,37] No obvious shift in the position of the reduced Zr^{4+} 3d bands was observed for both 0 HCl and 0.5 HCl coatings. For clarity, the fitted and extended Cl_{2p} bands are shown in Fig. 4(b). The satellite peaks of Zr^{4+} 3d band 195.6 eV were observed in all coatings. It was found the Cl_{2p} peak in the green and sintered 0.5 HCl coating

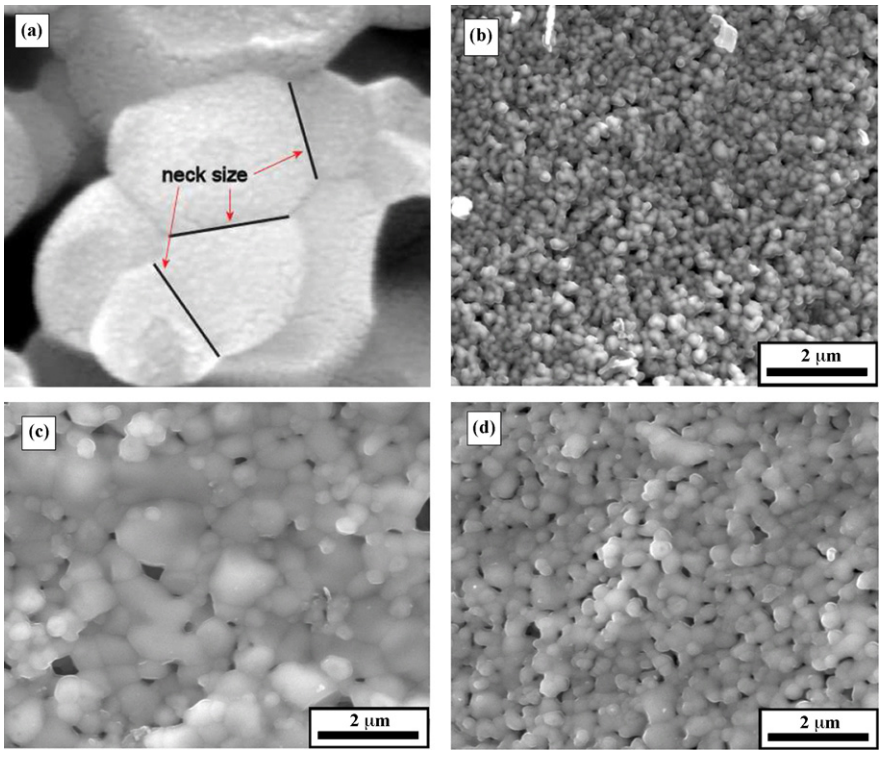

Fig. 2. (a) SEM image showing the procedure adopted to determine the grain size for all sintered coatings; (b) SEM image showing the surface morphology of green coating (HCl concentration = 0.5 mM); (c) surface morphology of 8YSZ coating (HCl concentration = 0.2 mM) after sintering at 1150 °C for 2 h; (d) surface morphology of 8YSZ coating (HCl concentration = 0.8 mM) after sintering at 1150 °C for 2 h.

partially overlapping with the satellite peak (see the top two curves in Fig. 4(b)).[38] For green and sintered 0.5 HCl coating, the Cl_{2p} peak at 197.7 eV corresponds to Zr–Cl which is a reaction product of HCl and Zr–OH.[39] In XPS spectra, the shift in peak position was expected as a strong electronegativity of Cl^- can cause the positions of Zr_{3d} and Y_{3d} to move towards a higher binding energy.[40,41]

Fig. 5(a) presents the atomic ratio of Cl_{2p}, Y_{3d} and reduced Zr^{4+} 3d to total Zr_{3d}, for green 0 HCl and 0.5 HCl 8YSZ coatings estimated from the XPS spectra (Fig. 4(a)).[31] Total Zr_{3d} is defined as the area sum of Zr $3d_{5/2}$, Zr $3d_{3/2}$ and reduced Zr^{4+} 3d bands. The reduced Zr^{4+} component represents 43% by area of the total Zr in the green 0 HCl coating (Fig. 5(a)). The presence of such a high amount of reduced Zr^{4+} indicates that the surface of the starting 8YSZ powder had a low degree of crystallization. This can be attributed to the presence of Zr–OH at the particle surface.[36] The Zr–OH rich surface of these 8YSZ particles possibly contributes to the low surface oxygen concentration, which could be partially oxidized after sintering at

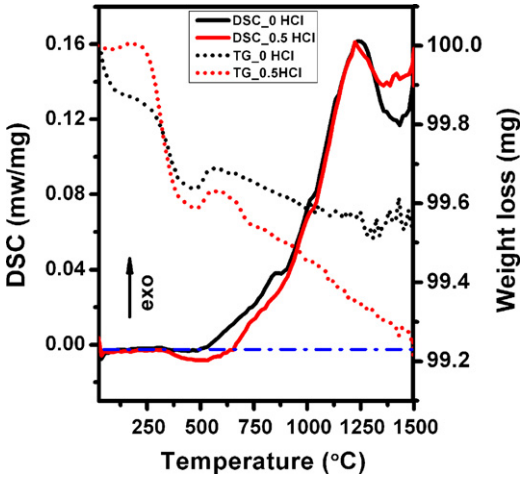

Fig. 3. Thermo-gravimetric (TG) and differential scanning calorimetric (DSC) behavior as function of calcination temperature for 0 HCl powder and 0.5 HCl 8YSZ powder.

Table 1
XPS bands of Zr_{3d}, reduced Zr^{4+} 3d, Y_{3d}, and Cl_{2p} in the 0 HCl and 0.5 HCl 8YSZ coatings before and after sintering at 1150 °C.

Band splitting	Binding energy (eV)			
	0 HCl coating		0.5 HCl coating	
	Green	Sintered	Green	Sintered
ZrO_2				
$3d_{5/2}$	181.2	181.2	182.9	182.4
$3d_{3/2}$	183.5	183.5	185.3	184.8
Reduced Zr^{4+} 3d	172.3	172.2	172.4	172.3
	174.7	174.4	174.7	174.8
Y_2O_3				
$3d_{5/2}$	156.0	156.0	158.1	157.4
$3d_{3/2}$	157.7	157.7	159.9	159.3
Cl 2p	–	–	197.7	197.7

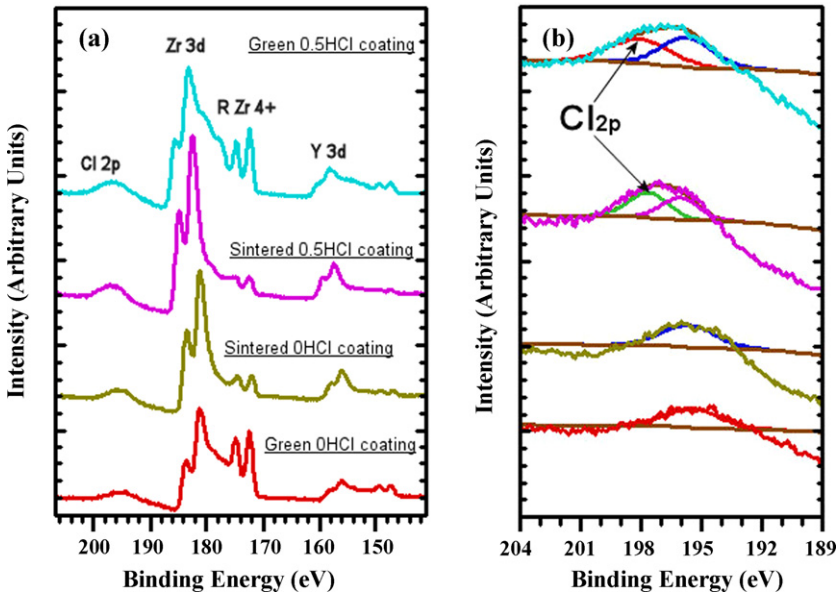

Fig. 4. (a) XPS spectra of green and 1150 °C – sintered 0 HCl and 0.5 HCl 8YSZ coatings; (b) XPS spectra of 2p bands of chlorine (Cl) for green and 1150 °C – sintered 0 HCl and 0.5 HCl 8YSZ coatings.

1150 °C.[42] The 0.16 atomic ratio of Y to Zr agrees well with the stoichiometric composition of starting 8YSZ power (8 mol% Y_2O_3 stabilized ZrO_2). For the green 0.5 HCl coating, a significant decrease in the atomic ratio of Y/Zr and reduced Zr^{4+}/Zr was observed as compared to the 0 HCl coating. Fig. 5(b) shows the atomic ratio of Cl_{2p}, Y_{3d} and reduced Zr^{4+} 3d to the total Zr_{3d}, for the sintered 0 HCl and 0.5 HCl 8YSZ coatings. As a proportion of the total Zr, about 15% and 7% of the reduced Zr^{4+} species remained in the 0 HCl and 0.5 HCl coatings after 1150 °C sintering, respectively (see Fig. 5(b)). A small increase in atomic ratio of Y/Zr was observed in both sintered 0 HCl and 0.5 HCl coating. The chlorine species remained in the sintered 0.5 HCl coating after 1150 °C sintering.

Fig. 6 shows the typical element distribution profile across the grain boundaries of 0 HCl and 0.5 HCl coating sintered at 1150 °C. It should be noted that detection of Cl in YSZ using X-ray analysis is hampered by the proximity of the Cl $K\alpha_{1,2}$ and Zr $L\alpha_{1,2}$ peaks at 2.62 and 2.04 keV respectively. Similarly detection of Cl by electron energy loss spectroscopy is hampered by the proximity of the loss edges for Cl $L_{2,3}$ and Zr $M_{4,5}$ at 200.00 eV and 180.00 eV respectively. The Cl species were detected in the sintered 0.5 HCl coating, and no detectable Cl species was found in the sintered 0 HCl coating. A marginal segregation of Cl species was present across the grain boundary in both coatings. The deficit of Y^{3+} ions and O^{2-} ions and the segregation of Zr^{4+} ions were clearly observed at the grain boundaries in the 0.5 HCl coatings as compared with the sintered 0 HCl coating which has no appreciable variation of elements across the grain boundary (Fig. 6(a)). Matsui et al.[19] reported that the grain growth in 8YSZ was much faster than that in 2YSZ and 3YSZ. The amount of segregated Y^{3+} ions in 8YSZ was significantly less than in 2YSZ and 3YSZ. This indicates that an increase in segregated Y^{3+} ions retards grain growth, which is consistent with our results.

4. Discussion

On introducing HCl into suspensions, a large fraction of Cl^- ions adsorbed on particle surface in green coatings. During sintering, the Cl^- ions was not formed in solid state solution but anchored onto the zirconia surface and trapped in pores as the charge and ionic radius of Cl^- ($r_{Cl^-} = 1.81$ Å) are too different from those of O^{2-} ($r_{O^{2-}} = 1.36$ Å).[22] A strong metal-oxide bond prevents the chlorine ions from deep penetration. The Cl_{2p} peak at 197.7 eV confirmed that chlorine was adsorbed on surface of particles in the green 0.5 HCl deposits (see Figs. 4 and 5).[39,40] A 43% proportion of the reduced Zr^{4+} species in the total Zr species, on the starting particle surface (Fig. 4a) favors interaction with Cl^- and results in $ZrCl_4$ or $ZrOCl_2$ formation.[20–22] The presence of Cl^- ions with a strong electro-negativity probably promoted Zr^{4+} and [Vö] migration to external surfaces and grain boundaries of YSZ to maintain electro-neutrality and resulted in the formation $ZrOCl_2$ and Cl·[Vö]·Cl.[39,40] In addition, the driving force for the surface migration of Zr^{4+} is the formation of strong chemical bonds with chloride. The standard formation molar enthalpy of crystalline $ZrCl_4$ is given[43] as; ΔH_f^0 ($ZrCl_4$, 298.15 K) = -980.7 ± 1.0 kJ mol^{-1}, which is more stable compound compared with other zirconium chloride compounds. Thus, the formation of $ZrCl_4$ on the surface of YSZ particles is energetically favored. The $ZrCl_4$ content increases with chloride ion concentration and independent of suspension pH value.[43] Consequently, $ZrCl_4$ and $ZrOCl_4$ interact with oxygen and ZrO_4 and Cl_2 is formed in the grain boundary which could result in Zr^{4+} and O^{2-} rich and Y^{3+} deficit in the grain boundary of 8YSZ. However, the grain boundaries in the sintered 0.5 HCl coating were depleted in O^{2-} (Fig. 6(b)) while no segregation or depletion of Cl was observed (Fig. 6(b)). This was consistent with a marginal decrease in atomic ratio of Cl/Zr which was observed

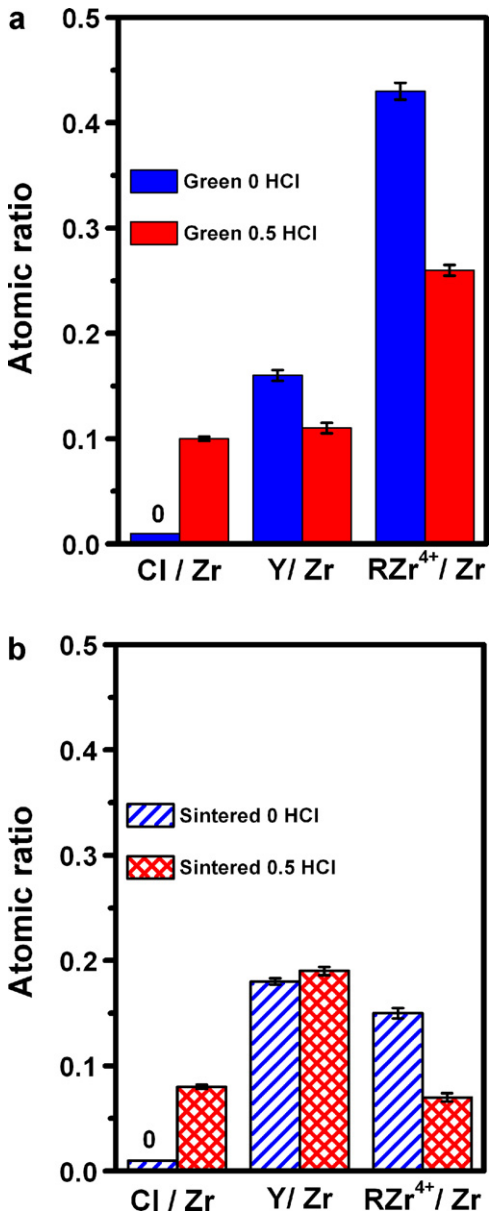

Fig. 5. The atomic ratio of Cl_{2p}, Y_{3d} and reduced Zr^{4+} 3d to total Zr_{3d} for 0 HCl and 0.5 HCl 8YSZ coating (a) before sintering; (b) after sintering at 1150 °C.

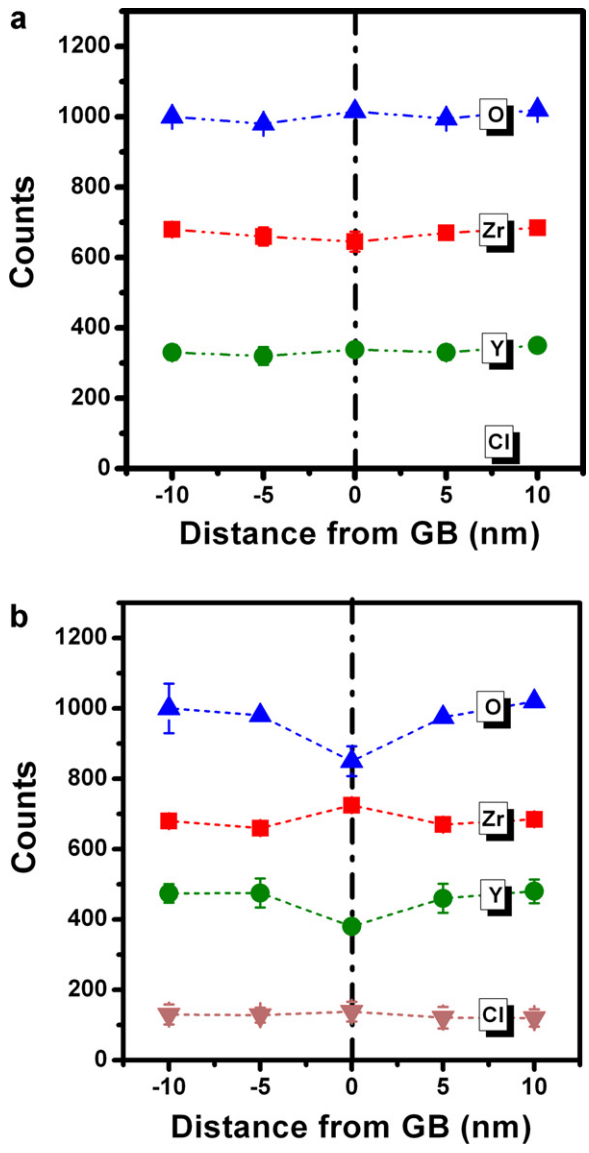

Fig. 6. Elements distribution profile across the grain boundaries of the sintered 8YSZ coating (a) 0 HCl coating; (b) 0.5 HCl coating.

in the sintered 0.5 HCl coating (Fig. 5). Thus, it is proposed that the segregation of oxygen vacancy [Vö] predominantly reduced the O^{2-} concentration in the grain boundary of 8YSZ in the sintered 0.5 HCl coating.

For YSZ solid solution, the oxygen vacancies prefer to associate with Zr^{4+} ions.[44] A strong electro-negativity of chlorine could drag Zr^{4+} ions and [Vö] to the surface and grain boundary of 8YSZ. Therefore, the presence of $ZrCl_4$, $ZrOCl_2$ and [Vö] segregation in the grain boundary could be responsible for large neck size to grain size ratio of 8YSZ coating with high HCl concentration. The oxidation of $ZrCl_4$ and $ZrOCl_2$ in the grain boundaries is beneficial for neck formation and growth because the formation of nano-sized ZrO_2 can lower the sintering temperature of 8YSZ.[45] The neck formation is predominated by the oxygen vacancy (Vö) diffusion for the 8YSZ due to low sintering activation energy as compared with Zr^{4+} cations.[46] The relation between the neck radius and diffusion coefficient of vacancies can be found from an equation proposed by Kuczynski.[13] He suggested that the neck size is proportional to sintering time and concentration of vacancies in the grain boundaries. The high oxygen vacancy concentration will lead to rapid neck growth. Thus, the presence of Cl^- ions on the 8YSZ grain could promote neck growth of 8YSZ in the 0.2, 0.5 and 0.8 HCl coatings (Fig. 1(b)) due to the presence of high oxygen vacancy concentration.

Substantial grain growth was expected for 0.2, 0.5 and 0.8 HCl coatings due to small amount of segregated Y^{3+} ions in grain boundary of 8YSZ.[19] Matsui et al.[19] found a rapid grain growth in 8YSZ compared with 2YSZ and 3YSZ. The amount of segregated Y^{3+} ions in 8YSZ was significantly less than in 2YSZ and 3YSZ. This indicates that an increase in segregated Y^{3+} ions retards grain growth due to the solute-drag mechanism

of Y^{3+} ions segregating along the grain boundary. In our case, marginal grain growth occurred in the 0.5 and 0.8 HCl coatings compared with 0.2 HCl coatings. The Y^{3+} segregation could not the reason to retard grain growth of 0.5 and 0.8 HCl coatings due to the deficit of Y^{3+} Consequently, the grain growth of 8YSZ grains in 0.2, 0.5 and 0.8 HCl coatings considerably depended on aggregate size[9,25,33] and marginally depend on the solute drag mechanism.[18,19]

5. Conclusions

In conclusion, we have investigated the effect of HCl concentration and particle packing on the sintering behavior of 8 mol% yttria-stabilized-zirconia (8YSZ) deposits. For different HCl concentrations, 8 mol% Y_2O_3 stabilized ZrO_2 (8YSZ) deposits were coated on metallic substrates using the electrophoretic deposition (EPD) method. It was found that the HCl concentration has a marked effect on the neck to grain size ratio of 8YSZ coating. For HCl concentration of 0.8 mM, the largest neck size to grain size ratio of 0.8 ± 0.03 was observed in 8YSZ coating. The grain growth of 8YSZ coating significantly depended on the initial aggregate size in the green EPD-coating. Using XPS, a Cl_{2p} band at 197.7 eV was observed in green and sintered 0.5 HCl coating. The position of Zr_{3d} bands and Y_{3d} bands in the green and sintered 0.5 HCl coatings appreciably shifted towards high binding energy as compared to the green and sintered 0 HCl coatings. Using STEM X-ray microanalysis, the deficit of Y^{3+} and O^{2-} ions, and the segregation of Zr^{4+} ions were clearly observed at the grain boundaries in sintered 0.5 HCl coatings as compared with the sintered 0 HCl coating. The presence of Cl^- ions in 0.2, 0.5 and 0.8 HCl YSZ coating could interact with Zr-OH on the surface of 8YSZ particles. The oxidation of resulting $ZrCl_4$ could lead to a Zr and oxygen vacancy [Vö] rich grain boundary because the Zr^{4+} and [Vö] would compensate the negative charge of adsorbed Cl^- ions on the grain surface of YSZ. The presence of $ZrCl_4$ and $ZrOCl_2$, and high concentration of oxygen vacancies in the grain boundaries promoted neck growth in the early stage sintering at 1150 °C. For low and high HCl concentration coatings, the difference in aggregate size and size distribution provided the main contribution to the difference in grain growth.

References

1. Garvie RC, Hannink RH, Pascoe RT. Ceramic steel. *Nature* 1975;**258**: 703–4.
2. Minh NQ. Ceramic fuel cells. *J Am Ceram Soc* 1993;**3**:563–88.
3. Zender HH, Leistner H, Searle HR. ZrO_2 materials for application in the ceramic industry. *Int Ceram* 1990;**39**:33–5.
4. Wang ZC, Shemilt J, Xiao P. Fabrication of composite coatings using a combination of electrochemical methods and reaction bonding process. *J Eur Ceram Soc* 2000;**20**:1469–73.
5. Wang ZC, Shemilt J, Xiao P. Fabrication of ceramic composite coatings using electrophoretic deposition, reaction bonding and low temperature sintering. *J Eur Ceram Soc* 2002;**22**:183–9.
6. Schlichting KW, Padture NP, Jordan EH, Gell M. Failure modes in plasma-sprayed thermal barrier coatings. *Mater Sci Eng A* 2003;**342**: 120–30.
7. Ji C, Lan W, Xiao P. Fabrication of yttria-stabilized zirconia coatings using electrophnoretic deposition: packing mechanism during deposition. *J Am Ceram Soc* 2008;**91**:1102–9.
8. Ji C, Shapiro IP, Xiao P. Fabrication of yttria-stablilized-zirconia coatings using electrophoretic deposition: effect of agglomerate size of distribution on particle packing. *J Eur Ceram Soc* 2009;**29**:3167–75.
9. Greskovich G, Lay KW. Grain growth in very porous Al_2O_3 compacts. *J Am Ceram Soc* 1972;**55**(3):142–6.
10. Lange FF, Kellett BJ. Thermodynamics of densification. II. Grain growth in porous compacts and relation to densification. *J Am Ceram Soc* 1989;**72**(5):735–41.
11. Shi JK, Deguchi Y, Sakabe Y. Relation between grain growth, densification and surface in solid state sintering—a direct observation. *J Mater Sci* 2005;**40**:5711–9.
12. Marco C, Rishi R. Surface diffusion-controlled neck growth kinetics in early stage intering of zirconia, with and without applied DC electrical field. *J Am Ceram Soc* 2011;**94**:391–5.
13. Kuczynski GC. Physics and chemistry of sintering. *Adv Colloid Interface Sci* 1972;**3**:275–330.
14. Perko S, Dakskobler A, Kosmac T. High-performance porous nanostructured ceramics. *J Am Ceram Soc* 2010;**93**(9):2499–502.
15. Lee IG, Chen IW. Sintering and grain growth in tetragonal and cubic zirconia. In: Somiya S, Shimada M, Yoshimura M, Watanabe R, editors. *Sintering'87*. London, UK: Elsevier Applied Science; 1988. p. 340.
16. Yoshizawa Y, Sakuma T. Role of grain-boundary glass phase on the superplastic deformation of tetragonal zirconia polycrystal. *J Am Ceram Soc* 1990;**73**(10):3069–73.
17. Sakuma T, Yoshizawa Y. The grain growth of zirconia during annealing in the cubic/tetragonal two-phase region. *Mater Sci Forum* 1992;**94**:865–70.
18. Ikuhara Y, Thavorniti P, Sakuma T. Solute segregation at grain boundaries in superplastic SiO_2-doped TZP. *Acta Mater* 1997;**45**:5275–84.
19. Matsui K, Yoshida H, Ikuhara Y. Grain-boundary structure and microstructure development mechanism in 2–8 mol% yttria-stabilized zirconia polycrystals. *Acta Mater* 2008;**56**:1315–25.
20. Matsui K, Ohgai M. Formation mechanism of hydrous-zirconia particles produced by hydrolysis of $ZrOCl_2$ solutions. II. *J Am Ceram Soc* 2000;**83**(6):1386–92.
21. Matsui K, Ohgai M. Formation mechanism of hydrous-zirconia particles produced by hydrolysis of $ZrOCl_2$ solutions. III. Kinetics study for the nucleation and crystal-growth processes of primary particles. *J Am Ceram Soc* 2001;**84**(10):2303–12.
22. Valigi M, Cimino A, Gazzoli D. The influence of additives (Cl^-, ReO_4^-, Ti(IV)) on some properties of ZrO_2. *Solid State Ionics* 1989;**32/33**: 698–705.
23. Shojai F, Mäntylä TA. Structural stability of yttria doped zirconia membranes in acid and basic aqueous solutions. *J Eur Ceram Soc* 2001;**21**:37–44.
24. Lawson S, Gill C, Dransfield GP. Hydrothermal and corrosive degradation of Y-TZP ceramics. *Key Eng Mater* 1995;**113**:207–14.
25. Readey MJ, Readey DW. Sintering of ZrO_2 in HCl Atmospheres. *J Am Ceram Soc* 1986;**69**(7):580–2.
26. Raether F, Springer R. In-situ Measurement of Neck formation during sintering of alumina by a novel thermo-optical measuring device. *Adv Eng Mater* 2000;**2**:741–4.
27. Suzuki M, Ikegami T, Yokoyama M. Effects of chloride ion densification transparency magnesia ceramics. *J Ceram Jpn* 2005;**113**(2): 149–53.
28. Parka HJ, Choab YH. The grain boundary conduction property of highly dense and nanostructured yttrium-doped zirconia. *Electrochem Solid-Stat Lett* 2010;**13**(5):K49–52.
29. Fullman RL. Measurement of particle sizes in opaque bodies. *Trans AIME* 1953;**197**(3):447–52.
30. Ardizzone S, Cattania MG, Lazzari P. Hydrothermal route to pure phase ZrO_2, Interfacial reactivity by XPS and electrochemical determinations. *Colloids Surf A: Physicochem Eng Aspects* 1994;**90**:45–54.
31. Badwal SPS, Hughes AE. The effect of sintering atmosphere on impurity phase formation and grain boundary resistivity in Y_2O_3-fully stabilized ZrO_2. *J Eur Ceram Soc* 1992;**10**:115–22.

32. Langford RM, Petford-Long AK. Preparation of transmission electron microscopy cross-section specimens using focused ion beam milling. *J Vac Sci Technol A* 2001;**19**(5):2186–93.
33. Guo FW, Shapiro IP, Xiao P. Effect of HCl on electrophoretic deposition of yttria stabilized zirconia particles in organic solvents. *J Eur Ceram Soc* 2011;**31**:2505–11.
34. Tojo T, Atake T, Mori T. Heat capacity and thermodynamic functions of zirconia and yttria-stabilized zirconia. *J Chem Thermodyn* 1999;**31**:831–45.
35. Yashima M, Ishizawa N, Yoshimura M. High-temperature X-ray study of the cubic–tetragonal diffusionless phase transition in the ZrO_2–$ErO_{1.5}$ system. II. Temperature dependence of oxygen ion displacement and lattice parameter of compositionally homogeneous 12 mol% $ErO_{1.5}$–ZrO_2. *J Am Ceram Soc* 1993;**76**(3):649–56.
36. Ram S, Mondal A. X-ray photoelectron spectroscopic studies of Al^{3+} stabilized t-ZrO_2 of nanoparticles. *Appl Surf Sci* 2004;**221**:237–47.
37. Tanabe T, Tanaka M, Imoto S. AES and XPS studies of oxygen stabilized alpha zirconium. *Surf Sci* 1987;**187**:499–510.
38. Sha L, Cho BO, Chang JP. Ion-enhanced chemical etching of ZrO_2 in a chlorine discharge. *J Vac Sci Technol A* 2002;**20**(5):1525–31.
39. Wren AG, Philips RW, Tolentino LU. Surface reactions of chlorine molecules and atoms with water and sulfuric acid at low temperatures. *J Colloid Interface Sci* 1979;**70**:544–57.
40. Dow WP, Huang TJ. Effect of chloride on TPR and TPO behaviour of an YSZ/(-Al_2O_3 supported copper oxide catalyst. *Appl Catal A: Gen* 1996;**141**:17–29.
41. Krzyzanowski S. The mechanism of the chemisorptions-induced segregation of titanium by chlorine in gold–titanium thin films. *J Mater Sci Lett* 1982;**1**:35–6.
42. Guo X. On the degradation of zirconia ceramics during low-temperature annealing in water or water vapor. *J Phys Chem Solids* 1999;**60**:539–46.
43. Efimov ME, Prokopenko IV, Medvedev VA. Thermodynamic properties of zirconium chlorides. II. The standard molar enthalpies of formation, the low-temperature heat capacities, the standard molar entropies, and the standard molar Gibbs energies of formation of zirconium monochloride, zirconium dichloride, and zirconium tetrachloride. *J Chem Thermodyn* 1989;**2**:677–85.
44. Li P, Chen IW. Effect of dopants on zirconia stabilization—an X-ray absorption study. I. Trivalent dopants. *J Am Ceram Soc* 1994;**77**(1): 118–28.
45. Baufeld B, Der Biesta OV, Rätzer-Scheibe HJ. Lowering the sintering temperature for EPD coatings by applying reaction bonding. *J Eur Ceram Soc* 2008;**28**(9):1793–9.
46. Suárez G, Garrido LB, Aglietti EF. Sintering kinetics of 8Y-cubic zirconia: cation diffusion coefficient. *J Mater Chem Phys* 2008;**100**:370–5.